Effect of lithiation on micro-scale fracture toughness of $Li_xMn_2O_4$ cathode

Muhammad Zeeshan Mughal [a], Riccardo Moscatelli [a], Hugues-Yanis Amanieu [b,c], Marco Sebastiani [a,*]

[a] Engineering Department, "Roma TRE" University, Via della Vasca Navale 79, 00146 Rome, Italy
[b] Institute for Materials Science and Centre for Nanointegration Duisburg–Essen (CENIDE), University of Duisburg–Essen, Universitatsstr. 15, 45141 Essen, Germany
[c] Robert BOSCH GmbH, Robert-Bosch-Platz 1, 70839 Gerlingen-Schillerhoehe, Germany

ARTICLE INFO

ABSTRACT

An optimized nanoindentation pillar splitting technique is used for the fracture toughness measurement of spinel $Li_xMn_2O_4$ cathode material under different states of charge (SoC), along with the high-speed nanoindentation results for nanomechanical property mapping. High-speed nanoindentation enables for a robust and efficient evaluation of elastic modulus and hardness as a function of the SoC on strongly heterogeneous materials. The fracture toughness decreases linearly upon de-lithiation, with an overall reduction of 53% from 0% to 100% SoC. Decrease in fracture toughness is associated with the volume change, increase of defect density and stresses related to diffusion of lithium upon de-lithiation.

© 2016 Elsevier Ltd. All rights reserved.

Lithium manganese oxide ($Li_xMn_2O_4$) is the most widely used cathode material in commercial Li-ion batteries because of its high voltage, low cost and environmental compatibility [1–3]. Over the lifetime of battery, Li intercalation and de-intercalation result in diffusion-induced strain as well as structural changes. In the case of $Li_xMn_2O_4$, this continuous removal and insertion of Li, due to diffusion, also brings a significant volume change, which induces the stresses and hence the onset of fracture [4]. Since key degradation mechanism in lithium ion batteries is usually associated with stress-induced mechanical failure, predicting the evolution of fracture toughness of the material upon cycling is an extremely critical issue, not yet solved, for controlling the performance and lifetime of these materials. The mechanical deformation in battery composites during electrochemical cycling is studied through various numerical models [5]; however, the quantitative utility of such models strongly depends upon the realistic measurements of elastoplastic and fracture properties, including toughness, as a function of lithium concentration in the electrode. Although there is plenty of literature which provides insight into the relationships among electrode microstructure, electro-chemical cycling, crystallographic changes in the active materials and resulting mechanical stresses, yet there are few reports on the composition dependency of the key physical properties [4,6]. In particular, no experimental quantitative and accurate measurements of fracture toughness evolution as a function of SoC have been reported so far, and hence provides a gap in understanding the extent to which fracture toughness and other elastoplastic properties of ion storage materials vary with lithium concentration.

In case of conventional indentation-based methods, the fracture toughness can be calculated from the measurement of crack lengths originating at the edges of micro-indentation impressions [7–9]. Reliability and accuracy of those methods is strongly related to the knowledge of crack geometry beneath the indentation mark and has been demonstrated to be a function of material properties and indenter geometry [7,10–13]. In addition, the presence of a compressive residual stress make it impossible to have crack growth in some cases [14,15].

Another approach involves the quantification of the energy dissipated during a pop-in event during the loading segment of a nanoindentation experiment [4,6]; such method requires the accurate measurement of the displacement associated to the pop-in event, which is extremely difficult to quantify due to artifacts coming from the dynamic response of the nanoindenter head [14,15]. In addition, the application to lithium-based composite electrodes is also challenging because of the significant influence of the surrounding soft/compliant matrix on the displacement that is measured during the test.

In the present report, a novel and relatively simple method for measuring the fracture toughness of lithium cathode micro-particles is used, which relies on sharp indentation testing on FIB-milled micro-pillars on the compact $Li_xMn_2O_4$ grains. The method does not require measurement

* Corresponding author.
  E-mail address: marco.sebastiani@uniroma3.it (M. Sebastiani).

of crack length, and substrate compliance effect is almost negligible, as demonstrated in recent papers [14,15]. Fracture toughness can be computed by only measuring the splitting load, pillar radius and hardness/modulus ratio of the material. The following equation shows the relationship used for calculating the fracture toughness values [14,15].

$$K_c = \gamma \frac{P_c}{R^{3/2}} \qquad (1)$$

where K_c is the fracture toughness (MPa·m$^{1/2}$), P_c is the critical load at failure by splitting (mN) and R is the pillar radius (μm). The coefficient γ is a material specific constant that has been recently evaluated for a wide range of materials' property combination by using Cohesive-Zone Finite Element Modeling (CZ-FEM). More details on the relationship, modeling and method applications can be found in author(s) previous publications [14,15].

Li$_x$Mn$_2$O$_4$-based cathode materials at different states of charge (SoC) are extracted from the commercial cells. The lattice parameter of each sample was determined by X-ray diffraction. This parameter has been demonstrated to be inversely proportional to lithiation in a previous publication [16]. The charging/discharging conditions for these samples, as well as extraction, polishing and XRD procedures are described elsewhere [16]. As mentioned in a previous paper [16], the experimentally calculated lattice parameter is smaller than the expected value for pristine spinal like LiMn$_2$O$_4$ sample (0.822–0.824 nm) [17,18]. It has been demonstrated previously, that not only the electrolyte decomposition at high voltage lowers the realistic deintercalation limit of Li ions, but also the oxygen molecules generated from charging activation reduced electrochemically, which can lead to extra discharge capacity [19] and lowers the realistic intercalation of Li [20]. For such reasons, the measured lattice parameter can be used to establish the evolution of the toughness upon lithiation, rather than the nominal SoC.

Literature modulus values for Li$_x$Mn$_2$O$_4$ composite cathodes vary from 80 GPa to 200 GPa and largely depend upon the indentation method, post-processing of the data as well as the condition of the sample (cathode material aged over time) [21–25]. In a recent paper, a statistical nanoindentation has been successfully applied to Li$_x$Mn$_2$O$_4$ composite cathodes [26]. Briefly, it involves taking several hundred indentations and filtering through various functions to separate the result of LiMn$_2$O$_4$ particles from the polymer matrix [26]. This process requires considerable post-processing of the data.

In this work, a novel high-speed nanoindentation mapping protocol is used. In contrast to standard quasi-static indentation mapping [26], this method allows to perform a significant number of complete load–unload experiments in a very small time [27]. In this way, maps with more than 3000 valid measurements with a penetration depth of 100 nm were performed in less than 1 h on strongly in-homogeneous battery composites. The tests were performed on a G200 Keysight nanoindenter equipped with express-test option and calibrated on a fused quartz reference sample. Finally, statistical deconvolution on the cumulative distribution functions of hardness and elastic modulus are performed [26]. No filtering tools were required in this case, because of the higher signal-to-noise ratio of the high-speed data, in comparison with the standard tests [26].

Pillars of ~5 μm diameter were milled using an FEI Helios Nanolab 600 focused ion beam (FIB) system [14]. The pillars were FIB milled in a single outer to inner pass using a current of 0.92 nA. For each sample, at least 5 pillars were milled on dense particles with the aspect ratio (h/D) of >1.2, where h is the pillar height and D is the top diameter. It has been shown previously that this method provides complete residual stress relaxation on the top surface of the pillars [28–30]. All pillar nano-indentation tests were performed using a Berkovich indenter using a strain rate of 0.05 s^{-1} [15]. The instrument frame stiffness and the indentation area function are calibrated on a certified fused quartz sample. As reported in a previous paper [16], the single particles are composed by multiple grains with an average size larger than 10 μm. In this paper, only 5 μm pillars produced inside a single-grain were considered for the fracture toughness experiments.
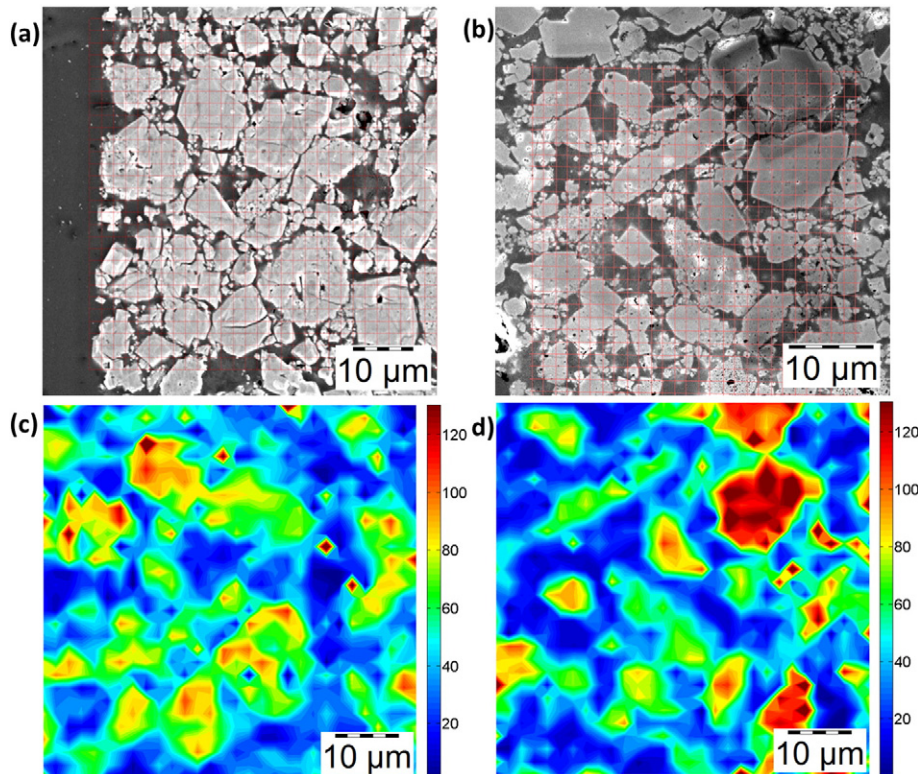
Fig. 1. (a) SEM micrograph highlighting the nanoindentation area for 0% SoC and (b) 100% SoC. (c–d) 2D nanoindentation modulus maps on the same areas (units in GPa) for (c) 0% SoC and (d) 100% SoC.
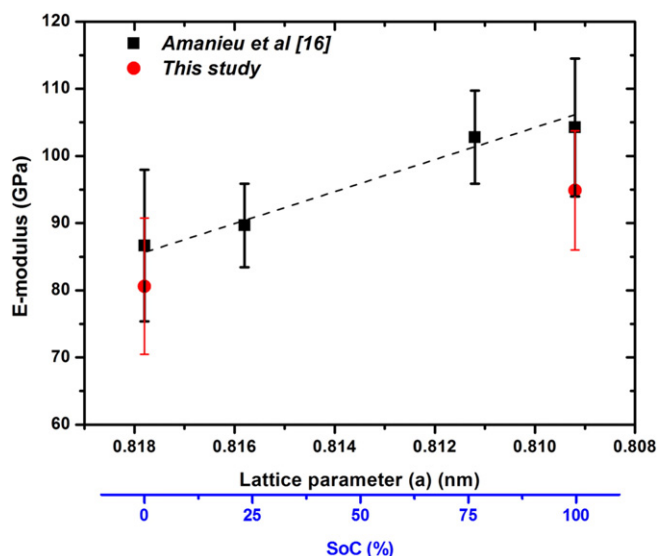
Fig. 2. Modulus variation with SoC using two different nanoindentation techniques. Lattice parameter data was taken from a previous publication [16].

Fig. 1a and b shows the SEM micrographs for the 0 and 100% SoC along with the statistical contour plots of elastic modulus (c, d), highlighting the area where high speed nanoindentation was carried out [31].

Fig. 2 shows the modulus values as a function of state of charge acquired through two different nanoindentation procedures. The data acquired using the standard nanoindentation procedure is shown as black squares and reported in author(s) previous publication [16]. The modulus values for 0 and 100% SoC acquired through express test are also shown in the same graph as red circles. The results are comparable

and are within the range of standard deviation. The observed minor difference between the two sets of data can be explained by the fact that our previous experiments involved the filtering procedure, while no filtering was applied to high-speed data. Nevertheless, the modulus values achieved through this method are very comparable with the ones reported in the previous publication.

Fig. 3 shows the representative images of the fractured pillar after nanoindentation as SoC. Different failure mode mechanisms are observed, in particular between fully charged and discharged samples. The analysis of fracture surfaces reveals that in fully discharge state, pillar split in number of fragments showing a small amount of plastic deformation and hence requires a higher energy to fracture. (Table 1). Looking at the SEM images of the split pillars, Fig. 3a–e, a continuous trend from damage-tolerant to fully brittle behavior is observed as a function of the SoC. An image of a pillar before splitting is also shown in Fig. 3d.

The load displacement curves obtained on pillars as a function of SoC% are presented in Fig. 4a. A clear and reproducible displacement burst is observed in all cases, due to unstable crack propagation in the pillars. One noticeable feature is that the loading segments are very reproducible up to a penetration depth of the order of 150 nm. Then, deviations are observed, probably due to substrate's effects during indentation of the stiff pillar over the compliant polymer matrix. As demonstrated in a previous paper [15], the effect of compliance substrate on the critical splitting load (which was ~11% in the worst case considered), can be corrected by evaluating specific values of γ coefficient in Eq. (1), by using ad-hoc CZ-FEM simulations [15]. Table 1 reports the experimental pillar radius, critical load at failure, the hardness and modulus values that were used for γ calculation and fracture toughness values of lithium ion battery samples under different states of charge.

Fig. 4b summarizes the results for the fracture toughness as the lattice parameter (and SoC) in $Li_xMn_2O_4$ cathode material. A very clear linear decrease of fracture toughness upon delithiation (charging) is
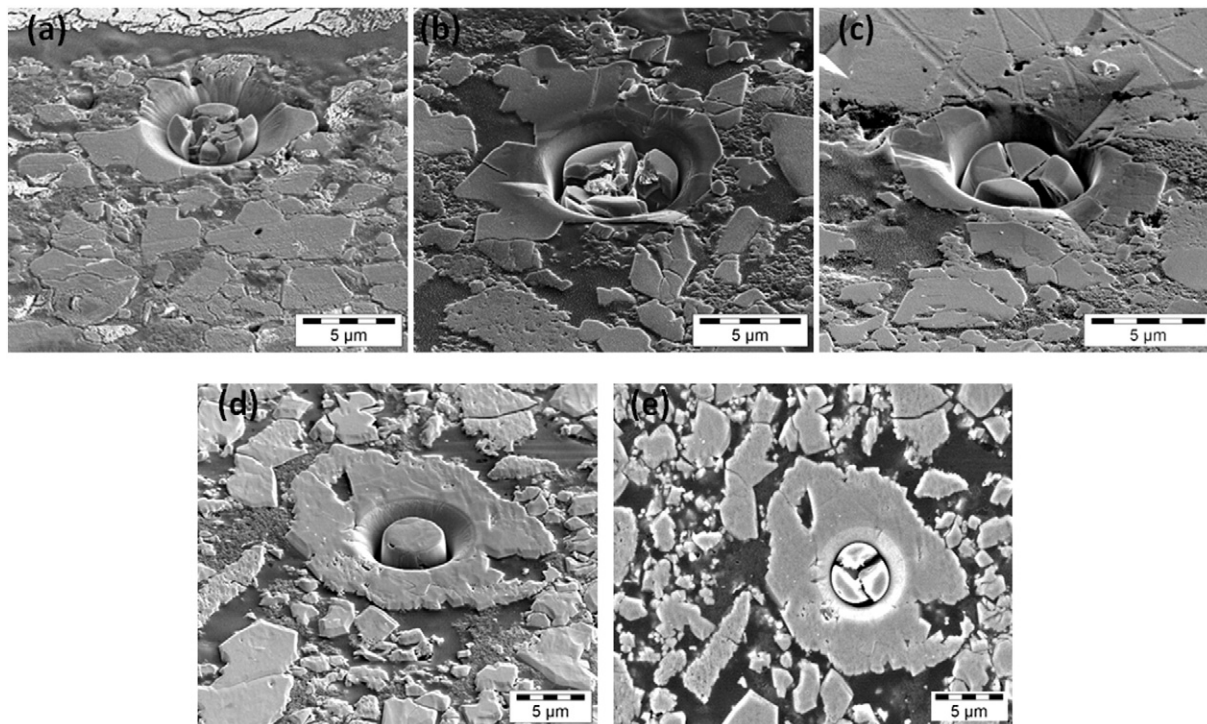

Fig. 3. FIB-milled micro-pillars after nanoindentation splitting with different SoC; (a) 0%, (b) 25% and (c) 75%. (d–e) Two images for 100%: FIB milled pillar (d) and after nanoindentation (e). All micrographs are acquired at 52° tilt (5 kV, SE, ETD, 5000×) except (e) which is taken at 0° tilt.

Table 1
Material properties and experimental results.

Nominal state of charge (SoC) %	0	25	75	100
Lattice parameter "a" (nm) [20]	0.8178	0.8158	0.8112	0.8092
Critical load at failure, L_c (mN)	8.33 ± 2.15	6.75 ± 1.31	5.07 ± 0.81	4.21 ± 0.46
Pillar radius, R (μm)	2.35 ± 0.1	2.35 ± 0.1	2.35 ± 0.1	2.35 ± 0.1
Experimental modulus, E (GPa)	86.67 ± 11.29	89.66 ± 6.23	102.78 ± 6.92	104.24 ± 10.26
Experimental hardness, H (GPa)	6.95 ± 0.76	6.51 ± 0.44	7.59 ± 0.62	7.95 ± 0.79
E/H	12.47	13.77	13.54	13.11
Substrate corrected finite element γ (Eq. (1))	0.212	0.229	0.229	0.221
Fracture toughness, K_c (MPa·m$^{1/2}$)	0.49 ± 0.13	0.43 ± 0.08	0.32 ± 0.05	0.26 ± 0.03

observed. From lithium ion battery stand point, the lithium concentration changes during charging and discharging and is known to change material properties, mostly the elastic modulus [4].

Recent works on lithiated silicon [32,33] and germanium [34] have shown a similar increase of fracture resistance after electrochemical lithiation, especially in the case of crystalline germanium, which shows the increase in fracture resistance upon lithiation due to the isotropic expansion. It is found that the germanium shows anisotropy in its lithiation-induced expansion and is due to the preferential lithiation along the <110> direction, they further explain that the increase in dimension along the <110> direction is 10% larger than the <100> direction. Despite of all these reports, a quantitative measurement of the effect of lithium content on fracture toughness was not possible, and this is the first time we systematically report the fracture toughness with the state of charge.

Fig. 4. (a) Representative load displacement curves of Li$_x$Mn$_2$O$_4$ with different SoC and (b) fracture toughness as a function of lattice parameter (a) in Li$_x$Mn$_2$O$_4$. Lattice parameter data was taken from a previous publication [16].

In the specific case of Li$_x$Mn$_2$O$_4$, the removal of Li during the delithiation process results in a proportional increase of Mn$^+$ ions in the particles; however, overall change in the elasto-plastic behavior depends upon the percentage of Mn^{3+} and Mn^{4+} ions. Lee et al. demonstrated that there are ten possible interactions involving; Li$^+$, Mn^{3+}, Mn^{4+} and O^{2-} ions during the charge and discharge [4]. Among various combinations, Mn^{4+}–Mn^{4+} interaction dominates at small SoC, while Mn^{+3}–O^{2-} and Li$^+$–O^{2-} interactions become important as the amount of Mn^{3+} increases as compared to Mn^{4+} ions. During the lithiation process (discharge), the percentage of Mn^{4+} increases as compared to the Mn^{3+} and since Mn^{4+}–O are stronger than Mn^{3+}–O, the ratio of Mn^{4+}/ Mn^{3+} will result in stiffer structure and hence the higher values of fracture toughness. This change can also be seen by the fact that the bond length is shorter and hence gives rise to a lower lattice parameter as reported by the XRD measurements [16] showing a regular decrease upon delithiation. This observation suggests that different concentrations of Mn^{4+} and Mn^{3+} ions upon lithiation play the major role during the cracking of the particles. Lee et al. further demonstrated that Mn^{4+}–O^{2-} interaction dominates the decline in the stress and the magnitude decreases as the value of x increases.
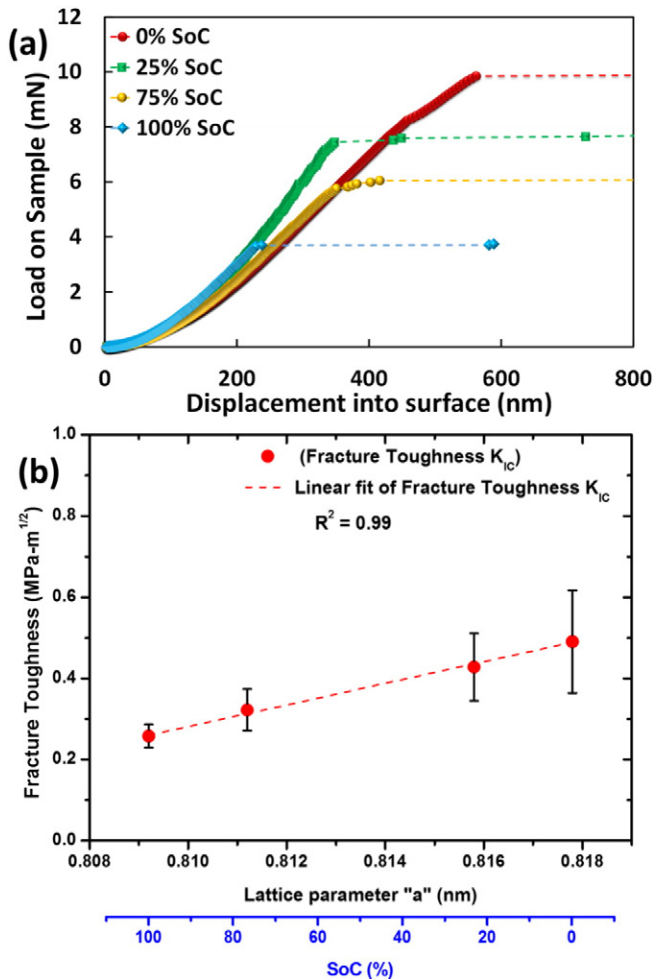
The effects of crystal anisotropy on fracture behavior may also have an effect on fracture behavior, which is not considered in this paper and will be the objective of future works.

Finally, the fracture toughness values obtained in this study for Li$_x$Mn$_2$O$_4$ spinal cathode material lie in the range of 0.26–0.49 MPa·m$^{1/2}$. Although there are no systematic literature reports on the analysis of fracture toughness of Li$_x$Mn$_2$O$_4$ to date, the calculated values can be compared to similar materials used in other studies. Jessica et al. uses Li$_x$CoO$_2$, as a cathode material and reported the fracture toughness values dropping from 1.0 MPa·m$^{1/2}$ to 0.3 MPa·m$^{1/2}$ upon charging [6]. Wolfenstein et al. reported the fracture toughness of Li-olivine cathodes (LiCoPO$_4$) between 0.4–0.5 MPa·m$^{1/2}$ [35]. Woodford et al. shows an electrochemical shock map to provide the fracture safety and fracture likely conditions, which strongly depend upon the particle size, they predicted the fracture toughness values in the range of 1–3 MPa·m$^{1/2}$ [22]. These literature reports are in good accordance with the fracture toughness values reported in the present study and provide an indirect confirmation of the results.

In conclusion, we have reported the fracture toughness values of Li$_x$Mn$_2$O$_4$ spinal cathode material, as a function of state of charge. The fracture toughness decreases as the SoC increases with an overall decrease of 53% from 0% SoC to 100% SoC, with a robust linear trend. The reason for the decrease is associated with the reduction of Li$^+$ and Mn^{4+} ions. The fracture toughness (~0.26–0.49 MPa·m$^{1/2}$) results are in very good agreement with the reported values of similar cathode materials. These change in fracture toughness values with respect to the state of charge could be really useful for micromechanical models to predict the life cycle and hence to improve the overall performance of these cathode materials.

Acknowledgments

References

[1] J.M. Tarascon, M. Armand, Nature 414 (2001) 359–367.
[2] J. Cabana, T. Valdés-Solís, M.R. Palacín, J. Oró-Solé, A. Fuertes, G. Marbán, A.B. Fuertes, J. Power Sources 166 (2007) 492–498.
[3] J. Park, J.H. Seo, G. Plett, W. Lu, A.M. Sastry, Electrochem. Solid-State Lett. 14 (2011) A14–A18.
[4] S. Lee, J. Park, A.M. Sastry, W. Lu, J. Electrochem. Soc. 160 (2013) A968–A972.
[5] A. Mukhopadhyay, B.W. Sheldon, Prog. Mater. Sci. 63 (2014) 58–116.
[6] J.G. Swallow, W.H. Woodford, F.P. McGrogan, N. Ferralis, Y.-M. Chiang, K.J. Van Vliet, J. Electrochem. Soc. 161 (2014) F3084–F3090.
[7] B.R. Lawn, A. Evans, D. Marshall, J. Am. Ceram. Soc. 63 (1980) 574–581.
[8] K.E. Johanns, J.H. Lee, Y.F. Gao, G.M. Pharr, Model. Simul. Mater. Sci. Eng. 22 (2014) 015011.
[9] T.L. Anderson, T. Anderson, Fracture Mechanics: Fundamentals and Applications, CRC Press, 2005.
[10] G. Anstis, P. Chantikul, B.R. Lawn, D. Marshall, J. Am. Ceram. Soc. 64 (1981) 533–538.
[11] J. Field, M. Swain, R. Dukino, J. Mater. Res. 18 (2003) 1412–1419.
[12] M. Laugier, J. Mater. Sci. Lett. 6 (1987) 355–356.
[13] T. Scholz, G. Schneider, J. Munoz-Saldana, M. Swain, Appl. Phys. Lett. 84 (2004) 3055–3057.
[14] M. Sebastiani, K. Johanns, E. Herbert, F. Carassiti, G. Pharr, Philos. Mag. (2014) 1–17.
[15] M. Sebastiani, K. Johanns, E. Herbert, G. Pharr, Curr. Opinion Solid State Mater. Sci. (2015).
[16] H.-Y. Amanieu, M. Aramfard, D. Rosato, L. Batista, U. Rabe, D.C. Lupascu, Acta Mater. 89 (2015) 153–162.
[17] K. Kanamura, H. Naito, T. Yao, Z.-i. Takehara, J. Mater. Chem. 6 (1996) 33–36.
[18] H. Berg, J. Thomas, Solid State Ionics 126 (1999) 227–234.
[19] N. Yabuuchi, K. Yoshii, S.-T. Myung, I. Nakai, S. Komaba, J. Am. Chem. Soc. 133 (2011) 4404–4419.
[20] T. Sui, B. Song, J. Dluhos, L. Lu, A.M. Korsunsky, Nano Energy 17 (2015) 254–260.
[21] M. Zhu, J. Park, A.M. Sastry, J. Electrochem. Soc. 159 (2012) A492–A498.
[22] W.H. Woodford, Y.-M. Chiang, W.C. Carter, J. Electrochem. Soc. 157 (2010) A1052–A1059.
[23] X. Zhang, A.M. Sastry, W. Shyy, J. Electrochem. Soc. 155 (2008) A542–A552.
[24] J. Christensen, J. Newman, J. Electrochem. Soc. 153 (2006) A1019–A1030.
[25] J. Park, W. Lu, A.M. Sastry, J. Electrochem. Soc. 158 (2011) A201–A206.
[26] H.-Y. Amanieu, D. Rosato, M. Sebastiani, F. Massimi, D.C. Lupascu, Mater. Sci. Eng. A 593 (2014) 92–102.
[27] J. Hay, P. Agee, Mapping the mechanical properties of alloyed magnesium (AZ 61), Source of the Document Conference Proceedings of the Society for Experimental Mechanics Series, 5 2014, pp. 97–101.
[28] A.M. Korsunsky, M. Sebastiani, E. Bemporad, Surf. Coat. Technol. 205 (2010) 2393–2403.
[29] M. Sebastiani, E. Bemporad, F. Carassiti, N. Schwarzer, Philos. Mag. 91 (2011) 1121–1136.
[30] M. Sebastiani, C. Eberl, E. Bemporad, G.M. Pharr, Mater. Sci. Eng. A 528 (2011) 7901–7908.
[31] M.Z. Mughal, R. Moscatelli, M. Sebastiani, Data in Brief, 2015.
[32] S.W. Lee, H.-W. Lee, I. Ryu, W.D. Nix, H. Gao, Y. Cui, Nat. Commun. 6 (2015).
[33] L.A. Berla, S.W. Lee, Y. Cui, W.D. Nix, J. Power Sources 273 (2015) 41–51.
[34] S.W. Lee, I. Ryu, W.D. Nix, Y. Cui, Extreme Mech. Lett. 2 (2015) 15–19.
[35] J. Wolfenstine, J.L. Allen, T.R. Jow, T. Thompson, J. Sakamoto, H. Jo, H. Choe, Ceram. Int. 40 (2014) 13673–13677.